Steel and Composite Structures, *Vol. 20, No. 2 (2016) 379-397*
DOI: http://dx.doi.org/10.12989/scs.2016.20.2.379

Long-term structural analysis and stability assessment of three-pinned CFST arches accounting for geometric nonlinearity

Kai Luo [a], Yong-Lin Pi [b], Wei Gao [*] and Mark A.Bradford [c]

Centre for Infrastructure Engineering and Safety, School of Civil and Environmental Engineering, University of New South Wales, Sydney, NSW 2052, Australia

(*Received February 23, 2015, Revised May 14, 2015, Accepted September 24, 2015*)

Abstract. Due to creep and shrinkage of the concrete core, concrete-filled steel tubular (CFST) arches continue to deform in the long-term under sustained loads. This paper presents analytical investigations of the effects of geometric nonlinearity on the long-term in-plane structural performance and stability of three-pinned CFST circular arches under a sustained uniform radial load. Non-linear long-term analysis is conducted and compared with its linear counterpart. It is found that the linear analysis predicts long-term increases of deformations of the CFST arches, but does not predict any long-term changes of the internal actions. However, non-linear analysis predicts not only more significant long-term increases of deformations, but also significant long-term increases of internal actions under the same sustained load. As a result, a three-pinned CFST arch satisfying the serviceability limit state predicted by the linear analysis may violate the serviceability requirement when its geometric nonlinearity is considered. It is also shown that the geometric nonlinearity greatly reduces the long-term in-plane stability of three-pinned CFST arches under the sustained load. A three-pinned CFST arch satisfying the stability limit state predicted by linear analysis in the long-term may lose its stability because of its geometric nonlinearity. Hence, non-linear analysis is needed for correctly predicting the long-term structural behaviour and stability of three-pinned CFST arches under the sustained load. The non-linear long-term behaviour and stability of three-pinned CFST arches are compared with those of two-pinned counterparts. The linear and non-linear analyses for the long-term behaviour and stability are validated by the finite element method.

Keywords: CFST arch; crown-pin; linear; non-linear; stability

1. Introduction

Concrete-filled steel tubular (CFST) arches are widely used in engineering structures, particularly in the bridge construction (Geng *et al*. 2012, Sundarraja and Ganesh Prabhu 2013, Han *et al*. 2014). The creep of the concrete core of a CFST arch occurs when a CFST arch is subjected to a sustained load and the shrinkage of the concrete core develops throughout the lifetime of the

*Corresponding author, Associate Professor, E-mail: w.gao@unsw.edu.au
[a] Ph.D. Student, E-mail: kai.luo@unsw.edu.au
[b] Professor, E-mail: y.pi@unsw.edu.au
[c] Scientia Professor, E-mail: m.bradford@unsw.edu.au

http://www.techno-press.org/?journal=scs&subpage=6 ISSN: 1229-9367 (Print), 1598-6233 (Online)

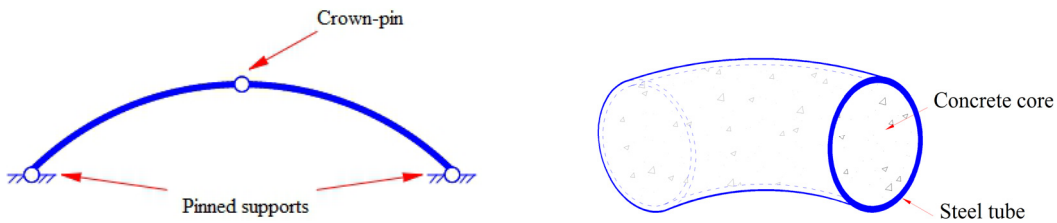

Fig. 1 Three-pinned arch with CFST section

arch even if it is not subjected to the external load. Owing to shrinkage and creep of the concrete core, deformations of a CFST arch under the sustained load continue to increase with time (Ma *et al*. 2011, Wang *et al*. 2011, Ma and Wang 2013, Mias *et al*. 2013). It is shown that creep and shrinkage have significant influence on structural behaviour of composite structures (Han *et al*. 2014, Al-Deen *et al*. 2015). In some cases, for construction convenience, arches are fabricated as two separate segments to reduce the arch size to meet transport requirements and then the two segments are joined together in the construction site (Fig. 1). The wet concrete is then placed into the steel tubes by high pressure pumping and it forms the concrete core after curing. The crown joint is often significantly weaker compared to the CFST arch-rib, and so it can be simplified structurally as a pin. The crown-pin is able to transfer shear forces and normal forces but is unable to resist bending moments, leading to free rotation of the arch segments about the pin, which makes the three-pinned arch statically determinate. Because of this, three-pinned arches are considered to be insensitive to environmental changes such as temperature and moisture, fabrication errors and support settlements.

Also because three-pinned CFST arches are statically determinate, it is conventionally thought that the linear analysis is sufficiently accurate in predicting their long-term structural behaviour, and it can be expected that linear analysis predicts the long-term deformations of three-pinned CFST arches, but does not predict the long-term changes of their internal actions (Gilbert and Ranzi 2011). However, it has been shown (Pi *et al*. 2011, Luo *et al*. 2013, 2015) that the long-term structural behaviour of CFST arches may be quite non-linear even under working loads. Because of the pin at the crown, the internal actions produced by the external loads in three-pinned CFST arches are quite different from those in two-pinned and fixed CFST arches, which may lead to quite different non-linear long-term structural behaviour and stability for three-pinned CFST arches. It has also been shown that to predict the in-plane structural behaviour and buckling load of three-pinned circular arches correctly, non-linear analysis is required. Therefore, in addition to the long-term linear analysis, knowledge about the non-linear long-term behaviour and stability of three-pinned CFST arches under sustained external loading is much needed.

This paper therefore presents a non-linear analysis of long-term structural behaviour and stability of three-pinned CFST circular arches under a sustained uniform radial load. The non-linear analysis is compared with its linear counterpart in predicting the long-term deformations, internal actions, and stability of three-pinned CFST arches. The effects of the crown-pin on the long-term structural behaviour and stability of three-pinned CFST arches will also be demonstrated by comparing with those of two-pinned CFST arches. This will provide an in-depth understanding of the non-linear long-term structural response and stability of three-pinned CFST arches.

A number of studies on long-term structural behaviour of straight CFST members have been reported (Uy 2001, Han *et al*. 2004, Wang *et al*. 2011, Chung *et al*. 2013, Ranzi *et al*. 2013). It is

known (Bazant and Cedolin 2003, Naguib and Mirmiran 2003, Wang *et al*. 2005, Shao *et al*. 2010, Gilbert and Ranzi 2011, Geng *et al*. 2012, Au and Si 2012, Ma and Wang 2013, Aslani 2015) that several methods can be used to model the creep and shrinkage of the concrete and have been used in investigations of the long-term responses of straight CFST members. It has been shown (Bradford *et al*. 2011, Pi *et al*. 2011) that the age-adjusted effective modulus method is effective and efficient in modeling the creep behaviour of the concrete core and it provides concise formulation in the non-linear analyses of statically indeterminate CFST structures such as two-pinned and fixed CFST arches. The age-adjusted effective modulus method is also recommended by ACI committee 209 (ACI 1982) and Australia Standard for Concrete Structures (AS3600 2009) and has been shown to be effective and feasible for the creep of concrete (Bazant and Cedolin 2003, Wang *et al*. 2005, Gilbert and Ranzi 2011). Hence, the age-adjusted effective modulus method is utilized in the present paper.

The linear and non-linear long-term analyses of CFST arches presented in this paper are based on the following common assumptions: (1) The Euler-Bernoulli hypothesis is adopted for the long-term deformations of the arch; (2) In consistence with the full bonding requirement of the construction specification for CFST arch bridges, the concrete core and the steel tube are assumed to be fully bonded so that no slip is allowed along their interface; (3) Arches are slender and the dimension of the cross-section is much smaller than the length and radius of the arch.

2. Linear analysis

In the design practice, linear analysis is usually thought to be sufficiently accurate for predicting the long-term structural responses of CFST structures. To facilitate the linear long-term analysis for three-pinned CFST arches under a uniform radial load q, the virtual work principle can be used to derive the differential equations of equilibrium for the long-term deformations. Because the arch and load system are symmetric, the statement of the virtual work principle for half of a CFST circular arch can be used for the derivation and it can be written as

$$\delta W = \int_{V_s} \sigma_s \delta\varepsilon \mathrm{d}V + \int_{V_c} \sigma_c \delta\varepsilon \mathrm{d}V - \int_0^{\Theta} qR^2 \delta\tilde{v} d\theta = 0 \quad \forall \quad \delta\tilde{v}, \delta\tilde{v}', \delta\tilde{v}'', \delta\tilde{w}, \delta\tilde{w}', \delta\varepsilon \tag{1}$$

where V_s and V_c are the volume of half of a CFST arch, $\delta\tilde{v}, \delta\tilde{v}', \delta\tilde{v}'', \delta\tilde{w}, \delta\tilde{w}'$ are kinematically admissible variation of deformations, $\delta\varepsilon$ is the variation of the compatible strain ε, θ is the angular coordinate, R is the radius of the circular arch, Θ is half of the included angle of the arch, and $\tilde{v}$

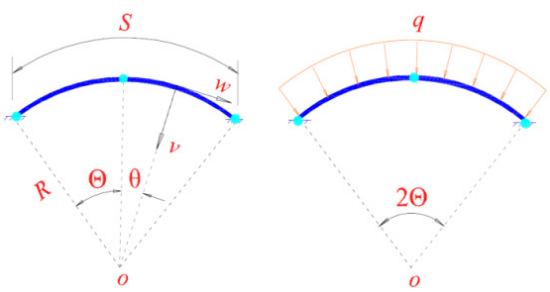

Fig. 2 Arch profile and the external load

and $\tilde{w}$ are dimensionless radial and axial displacements respectively, and are defined as $\tilde{v} = v/R$ and $\tilde{w} = w/R$, and ( )' ≡ d( )/dθ and ( )" ≡ d^2( )/dθ^2. For linear analysis, the linear strain ε_L can be used and it is given by (Pi *et al*. 2011, Luo *et al*. 2013, 2015)

$$\varepsilon_L = \tilde{w}' - \tilde{v} - \frac{y\left(\tilde{v}'' + \tilde{w}'\right)}{R} \quad . \tag{2}$$

Although the strain expression ε_L given by Eq. (2) is the same for the steel tube and concrete core, stresses σ_s in the steel tube and σ_c in the concrete core are different due to effects of creep and shrinkage of the concrete core, which can be expressed as (Pi *et al*. 2011, Luo *et al*. 2013, 2015)

$$\sigma_s = E_s \varepsilon_L \qquad \text{and} \qquad \sigma_c = E_{ec}(\varepsilon_L + \varepsilon_{sh}) \quad , \tag{3}$$

where the shrinkage strain ε_{sh} is a function of time t and is given by

$$\varepsilon_{sh}\left(t,d\right) = \left(\frac{t}{t+d}\right)\varepsilon_{sh}^{*} \tag{4}$$

with the final shrinkage strain ε_{sh}^{*} depending on the curing condition of the concrete and d = 35 days for the moist curing core concrete; and E_{ec} is the age-adjusted effective modulus of the concrete core given by

$$E_{ec}\left(t,t_0\right) = \frac{E_c}{1+\chi\left(t,t_0\right)\phi\left(t,t_0\right)} \quad , \tag{5}$$

in which t_0 is the time of initial loading, E_c is the elastic modulus of the concrete, $\phi(t,t_0)$ is the creep coefficient and $\chi(t, t_0)$ is the aging coefficient, which can be expressed (Gilbert and Ranzi 2011) as

$$\phi(t,t_0) = \frac{(t-t_0)^{0.6}\phi_u}{10+(t-t_0)^{0.6}} \tag{6}$$

and

$$\chi(t,t_0) = 1 - \frac{(1-\chi^{*})(t-t_0)}{20+(t-t_0)} \quad , \tag{7}$$

where the final creep coefficient ϕ_u and aging coefficient χ^{*} are given by

$$\phi_u = 1.25 t_0^{-0.118}\phi_{\infty,7} \ , \quad \text{and} \quad \chi^{*} = \frac{k_1 t_0}{k_2 + t_0} \quad \text{with} \quad \begin{cases} k_1 = 0.78 + 0.4e^{-1.33\phi_{\infty,7}} \\ k_2 = 0.16 + 0.8e^{-1.33\phi_{\infty,7}} \end{cases} . \tag{8}$$

By integrating the virtue work statement given by Eq. (1) by parts, linear differential equations of equilibrium in the radial and axial directions can be derived as

$$r_e^2\left(\tilde{v}^{iv} + \tilde{w}'''\right) - R^2\left(\tilde{w}' - \tilde{v}\right) - \frac{A_c E_{ec}\varepsilon_{sh}R^2 + qR^3}{A_s E_s + A_c E_{ec}} = 0 \tag{9}$$

and

$$r_e^2\left(\tilde{v}''' + \tilde{w}''\right) + R^2\left(\tilde{w}'' - \tilde{v}'\right) = 0\,, \tag{10}$$

and the static boundary conditions can be derived at the same time as

$$\tilde{v}'' + \tilde{w}' = 0 \quad \text{at} \quad \theta = 0 \quad \text{and} \quad \theta = \pm\Theta\,. \tag{11}$$

In Eqs. (9) and (10), r_e is the time-dependent radius of gyration of the effective cross-section about its major principle axis and is defined as

$$r_e = \sqrt{\frac{E_s I_s + E_{ec} I_c}{A_s E_s + A_c E_{ec}}}\,. \tag{12}$$

The solutions of the differential equations of equilibrium given by Eqs. (9) and (10) need to satisfy the static boundary conditions given by Eq. (11) and the essential kinematic boundary conditions for three-pinned arches given by

$$\tilde{v} = 0 \text{ at } \theta = \pm\Theta \text{ and } \tilde{w} = 0 \text{ at } \theta = 0,\ \pm\Theta\,. \tag{13}$$

The solutions for the dimensionless linear radial displacement $\tilde{v}$ and axial displacement $\tilde{w}$ can then be obtained as

$$\tilde{v} = \frac{qR + A_c E_{ec}\varepsilon_{sh}}{A_s E_s + A_c E_{ec}}\left[1 + \cos\theta - \mathrm{H}(\theta)\frac{\sin\theta\sin\Theta}{1-\cos\Theta}\right] \tag{14}$$

and

$$\tilde{w} = \frac{qR + A_c E_{ec}\varepsilon_{sh}}{A_s E_s + A_c E_{ec}}\left[\sin\theta - \mathrm{H}(\theta)\frac{(1-\cos\theta)\sin\Theta}{1-\cos\Theta}\right], \tag{15}$$

where H(θ) is the step function defined by

$$\mathrm{H}(\theta) = \begin{cases} -1 & \text{when } \theta < 0 \\ 1 & \text{when } \theta \geq 0 \end{cases}. \tag{16}$$

The typical distributions of the long-term radial displacements given by Eq. (14) are shown in Fig. 3 for a three-pinned CSFT arch with a span L = 15m consisting of the circular steel tube and concrete core with the steel tube having inner and outer radii r_i = 0.24 m and r_o = 0.25 m. In the calculation of the long-term displacements, proper values for the final creep coefficient and final shrinkage strain need to be determined first. Although several experimental investigations on the final creep coefficient and final shrinkage strain have been reported (Terrey *et al*. 1994, Uy 2001, Ichinose *et al*. 2001, Han *et al*. 2004), the test results depend upon the quality of concrete and the environmental conditions and have large discrepancies among these investigations (Mirza and Uy 2010, Ahmed and Sobuz 2011). For convenience of calculation, the results derived from the experimental results of Uy (2001) *viz*. final creep coefficient ϕ_u = 2.27 ($\phi_{\infty,7}$ = 2.5) and the final shrinkage strain ε_{sh}^* = 340 × 10^{-6} are adopted in the present investigation.

The arches are assumed to be subjected to a uniform radial load $qR = 0.5N_{cr}$, where N_{cr} is the

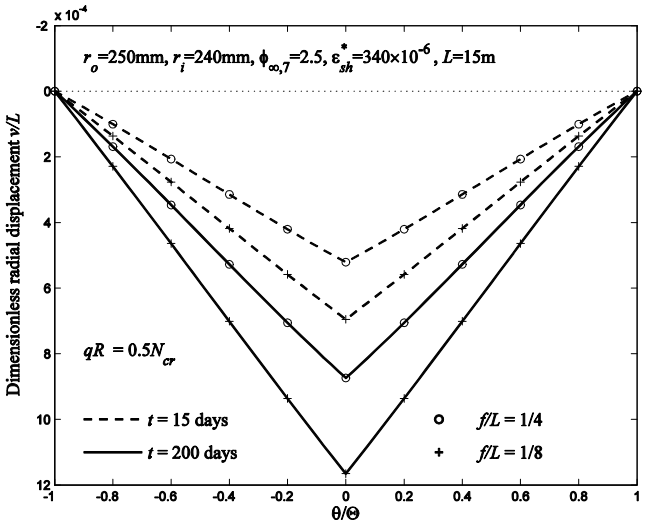

Fig. 3 Distributions of long-term radial displacements

second mode flexural buckling load of pin-ended CFST columns with the same cross-section and the same span of L = 15 m under uniform axial compression at time t_0 = 15 days and given by

$$N_{cr} = \frac{\pi^2 (E_s I_s + E_{ec} I_c)}{(L/2)^2}. \tag{17}$$

It can be seen from Fig. 3 that linear analysis predicts significant increases of the radial displacements from time t = 15 days to time t = 200 days for both arches with the rise-to-span ratio f/L = 1/4 and f/L = 1/8. This indicates that the serviceability limit state of a three-pinned CFST arch that is satisfied in the short-term ($v < L/1000$, where deflection limit $L/1000$ is assumed) may be violated in the long-term ($v > L/1000$ for the arch with f/L = 1/8).

By substituting the solutions of the dimensionless linear radial and axial displacements, the linear axial force N and bending moment M can be obtained as

$$N = -(A_s E_s + A_c E_{ec})(\tilde{w}' - \tilde{v}) - \varepsilon_{sh} A_c E_{ec} = qR \tag{18}$$

and

$$M = -(E_s I_s + E_{ec} I_c)\frac{\tilde{v}'' + \tilde{w}'}{R} = 0. \tag{19}$$

Eqs. (18) and (19) show that linear analysis does not predict long-term changes of the internal forces, which indicates that the creep and shrinkage of the concrete core do not influence the internal forces in the long-term because three-pinned CFST arches are statically determinate. This is consistent with Gilbert and Ranzi (2011).

The three-pinned CFST arch may buckle in the long-term if the sustained uniform radial load is sufficiently high and the time is sufficiently long. Based on the short-term linear buckling load proposed by Schmidt (1979), the long-term linear buckling load q_{cr} of three-pinned CFST arches can be expressed as

Table 1 Coefficient K

2Θ	30°	60°	90°	120°	150°	180°
K	108.36	27.077	12.025	6.758	4.322	3.000

Table 2 Linear long-term buckling loads of three-pinned CFST arches

Time t (days)	Included angle 2Θ	Linear buckling $q_{cr}R/N_{cr}$	
		Analytical solutions	Finite element results
15	30	0.753	0.744
	60	0.752	0.751
	90	0.752	0.751
	120	0.751	0.751
	150	0.750	0.750
	180	0.750	0.750
400	30	0.551	0.544
	60	0.551	0.550
	90	0.550	0.550
	120	0.550	0.550
	150	0.549	0.550
	180	0.549	0.549

$$q_{cr} = K\frac{E_s I_s + E_{ec} I_c}{R^3} \tag{20}$$

where the factor K is given in Table 1.

The linear long-term buckling loads of a group of three-pinned CFST arches given by Eq. (20) are listed in Table 2. It can be seen that although the linear analysis does not predict any changes of the internal forces for three-pinned CFST arches, it predicts that three-pinned CFST arches may buckle in the long-term and that the linear long-term buckling loads vary little with the included angle. The finite element (FE) results for the linear long-term buckling loads obtained from a FE program for the time-dependent analysis of CFST structures in association with ANSYS (2006) developed by authors elsewhere (Luo *et al*. 2013, 2015) are also shown in Table 2. The agreements between the analytical solutions given by Eq. (20) and the FE results are very good.

3. Non-linear analysis

It has been shown that the linear analysis is not adequate in predicting the short-term structural behaviour and stability of three-pinned arches and non-linear analysis is required for correct predictions. Hence, geometric nonlinearity may also need to be considered in the long-term analysis of three-pinned CFST arches. For non-linear long-term analysis, the strain ε needs to account for the non-linear term $(\tilde{v}')^2/2$ and can be expressed as (Pi *et al*. 2002, Luo *et al*. 2015)

$$\varepsilon = \tilde{w}' - \tilde{v} + \frac{1}{2}\tilde{v}'^2 - \frac{y\tilde{v}''}{R}. \tag{21}$$

By substituting Eq. (21) into Eq. (1) and integrating it by parts, the differential equations of equilibrium in the axial and radial directions for non-linear long-term analysis can be derived as

$$N' = 0 \quad \text{and} \quad \frac{\tilde{v}^{iv}}{\mu_e^2} + \tilde{v}'' = P, \tag{22}$$

and at the same time, the static boundary conditions can also be derived as

$$\tilde{v}'' = 0 \quad \text{at} \quad \theta = 0 \quad \text{and} \quad \theta = \Theta \tag{23}$$

and

$$\tilde{v}''' + \mu_e^2 \tilde{v}' = 0 \quad \text{at} \quad \theta = 0 \tag{24}$$

In Eqs. (22) and (24), μ_e is a time-dependent dimensionless axial force parameter and P is a dimensionless load and they are defined as

$$\mu_e^2 = \frac{NR^2}{E_s I_s + E_{ec} I_c} \quad \text{and} \quad P = \frac{qR}{N} - 1, \tag{25}$$

where N is the axial compressive force and given by

$$N = -\int_A \sigma dA = -\left(A_s E_s + A_c E_{ec}\right)\left[\tilde{w}' - \tilde{v} + \frac{1}{2}\left(\tilde{v}'\right)^2\right] - A_c E_{ec} \varepsilon_{sh}. \tag{26}$$

In addition, the essential kinematic boundary conditions given by

$$\tilde{w} = 0 \quad \text{at} \quad \theta = 0 \quad \text{and} \quad \theta = \Theta, \text{ and } \tilde{v} = 0 \quad \text{at} \quad \theta = \Theta \tag{27}$$

also need to be satisfied.

Solving the second equation of Eq. (22) under the boundary conditions given by Eqs. (23), (24) and (27) leads to the dimensionless long-term radial displacement $\tilde{v}$ as

$$\tilde{v} = \frac{P}{\mu_e^2}\left[\cos\mu_e\theta - 1 + \mathrm{H}(\theta)\sin\mu_e\theta \tan\frac{\beta_e^2}{2} + \frac{1}{2}\left(\mu_e^2\theta^2 - \beta_e^2\right)\right] \tag{28}$$

where the new time-dependent axial force parameter β_e is defined by $\beta_e = \mu_e\Theta$.

It can be seen from Eqs. (25) and (28) that the long-term radial displacements $\tilde{v}$ is a function of the dimensionless load P and the time-dependent axial force parameter $\mu_e(\beta_e)$. Hence, to evaluate the long-term radial displacement, the relationship of the dimensionless load P with the time-dependent parameters $\beta_e(\mu_e)$ need to be established. From the first equation of Eq. (22), the axial compressive force N is a constant along the arch. Considering this and substituting Eq. (28) into Eq. (26) and integrating its both sides over the entire arch (from $-\Theta$ to Θ) leads to a quadratic equation of equilibrium between P and β_e as

$$A_1 P^2 + B_1 P + C_1 = 0 \tag{29}$$

where the coefficients A_1, B_1, and C_1 are given as

$$A_1 = \frac{1}{\beta_e^2}\left[1 - \frac{5\sin\beta_e - \beta_e}{2\beta_e(1+\cos\beta_e)}\right] + \frac{1}{6}, \tag{30}$$

$$B_1 = \frac{1}{\beta_e^2}\left[1 - \frac{2\sin\beta_e}{\beta_e(1+\cos\beta_e)}\right] + \frac{1}{3}, \tag{31}$$

and

$$C_1 = \frac{\beta_e^2}{\lambda_e^2} + \frac{A_c E_{ec} \varepsilon_{sh}}{\Theta^2 (A_s E_s + A_c E_{ec})}, \tag{32}$$

with the time-dependent geometric parameter λ_e being defined as

$$\lambda_e = \frac{R\Theta^2}{r_e}. \tag{33}$$

The non-linear long-term bending moment M can then be obtained as

$$M = -\frac{(E_s I_s + E_{ec} I_c)\tilde{v}''}{R} = -\frac{P(E_s I_s + E_{ec} I_c)}{R}\left[1 - \cos\mu_e\theta - \mathrm{H}(\theta)\sin\mu_e\theta\tan\frac{\beta_e}{2}\right]. \tag{34}$$

4. Non-linear long-term analysis

4.1 Long-term non-linear deformations

From Eq. (29), the long-term axial compressive force N (through the parameter β_e) of a CFST arch is a non-linear function of the dimensionless load P. For a given CFST arch under a given dimensionless sustained load P at a given time t, solving Eq. (29) can produce the dimensionless long-term axial force parameter β_e. Subsequently, substituting the obtained $\beta_e(\mu_e)$ and P into Eq. (28) results in the long-term radial displacement v, and substituting $\beta_e(\mu_e)$ and P into Eq. (34) results in the long-term bending moment M.

Typical distributions of the non-linear long-term radial displacements v/f and bending moments $8M/qS^2$ along the length of the arch so obtained are shown in Figs. 4a and 4b for the same arches used in the linear analysis but with a sustained uniform radial load $qR = 0.3N_{cr}$, where S is the length of the arch. For comparison, the distributions of the dimensionless linear long-term radial displacements given by Eq. (14) under the same load are also shown in Fig. 4(a).

It can be seen from Fig. 4(a) that non-linear analysis predicts much larger short and long-term radial displacements than the linear analysis. This indicates that when the geometric nonlinearity is considered, the serviceability limit state of a three-pinned CFST arch that is satisfied in the short-term may be violated in the long-term. It can also be seen from Fig. 4(b) that linear analysis predicts zero bending moment while the non-linear analysis predicts significant short-term and

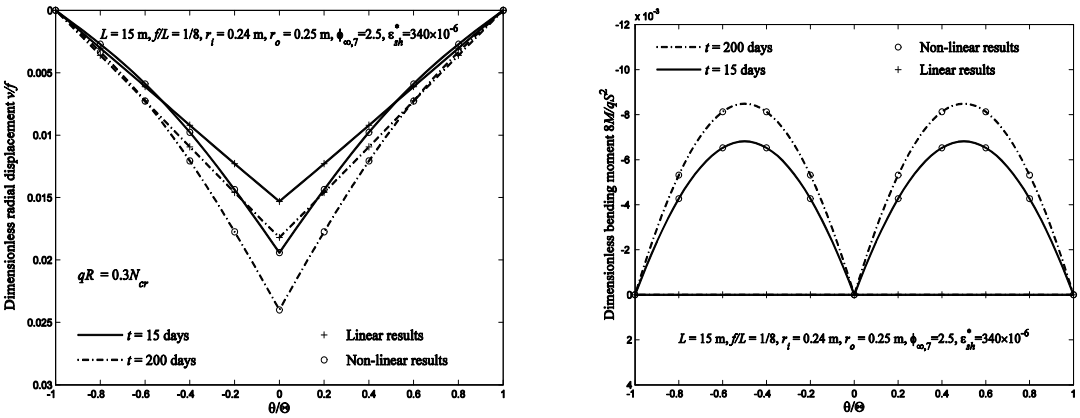

(a) Distributions of radial displacements (b) Distributions of bending moments

Fig. 4 Distributions of non-linear long-term radial displacements and bending moments

long-term bending moments. The increase of the bending moment may also influence the in-plane stability of the three-pinned CFST arch in the long-term.

The influence of geometric nonlinearity on the long-term deformations of three-pinned CFST arches is also shown in Fig. 5 as the history of the dimensionless long-term central radial displacement $v_c/v_{c,15}$ where $v_{c,15}$ is the central radial displacement at t_0 = 15 days and the arch is subjected to a sustained uniform load $qR = 0.2\,N_{cr}^s$, where N_{cr}^s is the second mode flexural buckling load of pin-ended CFST columns with the same cross-section and the same length S under uniform axial compression at time t_0 = 15 days and given by

$$N_{cr}^s = \frac{\pi^2 (E_s I_s + E_{ec} I_c)}{(S/2)^2}. \tag{35}$$

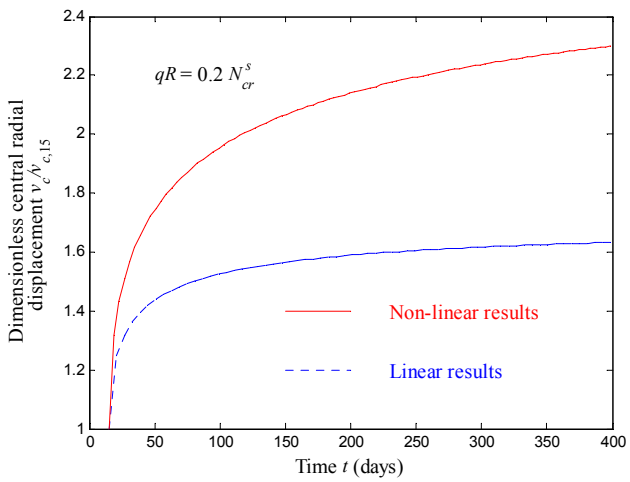

Fig. 5 Dimensionless long-term central radial displacement $v_c / v_{c,15}$

It can be seen that at time t = 50 days, the linear long-term central displacement is $v_c \approx 1.44v_{c,15}$, while the non-linear long-term central displacement is $v_c \approx 1.74v_{c,15}$. At the time t =400 days, the linear long-term central displacement is $v_c \approx 1.63v_{c,15}$, while the non-linear long-term radial displacement $v_c \approx 2.30v_{c,15}$. This shows again that the influence of geometric nonlinearity on the long-term radial displacements of three-pinned CFST arches is significant and needs to be considered in the long-term analysis.

4.2 Long-term equilibrium and buckling behaviour

The equation of equilibrium between the dimensionless load P and the axial compressive force parameter β_e given by Eq. (29) in conjunction with the radial displacement $\tilde{v}$ given by Eq. (28) describes the non-linear equilibrium of a three-pinned CFST arch. Typical non-linear equilibrium paths of a three-pinned CFST arch (f/L = 1/20 and L = 15 m) at time t =15, 50, 200, and 400 days are shown in Figs. 6(a)-6(d) as variations of the dimensionless uniform radial load qR/N_{cr}^{s} with the dimensionless central radial displacement v_c/f.

It can be seen that the radial displacements increase non-linearly with an increase of the uniform radial load until a limit point is reached. At the limit point, any further small increase of the uniform radial load will cause the arch to lose its stability and snap through to its remote equilibrium branch, i.e., limit point (snap-through) buckling occurs. It can also be seen from Figs. 6a-6d that at different times the CFST arch has different equilibrium paths and the buckling load decreases substantially with time because of the creep and shrinkage effects of the concrete core. Under the sustained load $qR = 0.2095\ N_{cr}^{s}$, the arch does not buckle at time t = 15, 50 and 200 days (Fig. 6(a)-6(c)), but it buckles at time t = 400 days as shown in Fig. 6(d). This means that when the uniform radial load increases to the value $qR = 0.2095\ N_{cr}^{s}$ at time t = 15 days, the CFST arch does

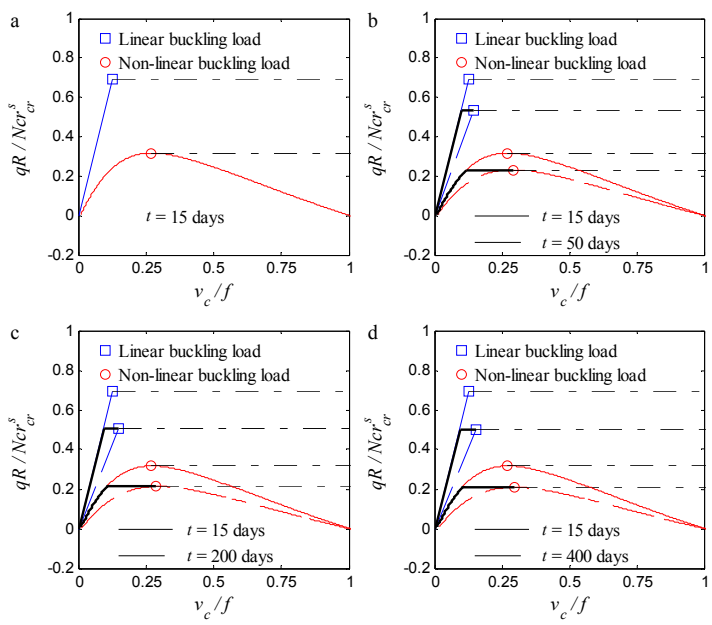

Fig. 6 Equilibrium and buckling of a three-pinned CFST arch at different times

Table 3 Comparison of linear and non-linear buckling load

qR	t = 15 days	t = 50 days	t = 200 days	t = 400 days
Non-linear	0.3172 N_{cr}^{s}	0.2319 N_{cr}^{s}	0.2141 N_{cr}^{s}	0.2095 N_{cr}^{s}
Linear	0.6913 N_{cr}^{s}	0.5347 N_{cr}^{s}	0.5055 N_{cr}^{s}	0.4972 N_{cr}^{s}

not buckle instantaneously. However, if the load is sustained until t = 400 days, it happens to be equal to the limit buckling load at t = 400 days (Fig. 6(d)), the CFST arch will buckle in the snap-though mode. The non-linear buckling loads of the CFST arch at different times are also listed in the first row of Table 3.

For comparison, the linear equilibrium paths given by Eq. (14) and buckling loads given by Eq. (20) are also shown in Fig. 6 and Table 3. It can be seen from Fig. 6 that the linear radial displacements are smaller than their non-linear counterparts under the same load while the linear buckling loads are much higher than their non-linear counterparts. It can also be seen from Table 3 that the three-pinned CFST arch under the sustained load qR = 0.4 N_{cr}^{s} does not buckle in both the short-term (t =15 days) and the long-term (t = 400 days) according to the linear predictions, but does buckle in both the short-term and the long-term according to the non-linear predictions.

In order to verify the analytical solutions for the non-linear equilibrium paths given by Eqs. (28) and (29), a FE program for the long-term analysis of CFST structures in association with ANSYS (2006) developed by authors elsewhere (Luo *et al*. 2013, 2015) was used in the present paper to perform non-linear analyses for three-pinned CFST arches. The FE results for the non-linear equilibrium paths at the time t = 15 days, 200 days and 400 days are compared with the analytical solutions in Fig. 7 as variations of the dimensionless load qR / N_{cr}^{s} with dimensionless central radial displacements v_c/f, where the circles represent the FE results and solid line represents the analytical solutions. It can be seen that the non-linear analytical solutions for the long-term behaviour of three-pinned CFST arches agree with their FE counterparts extremely well.

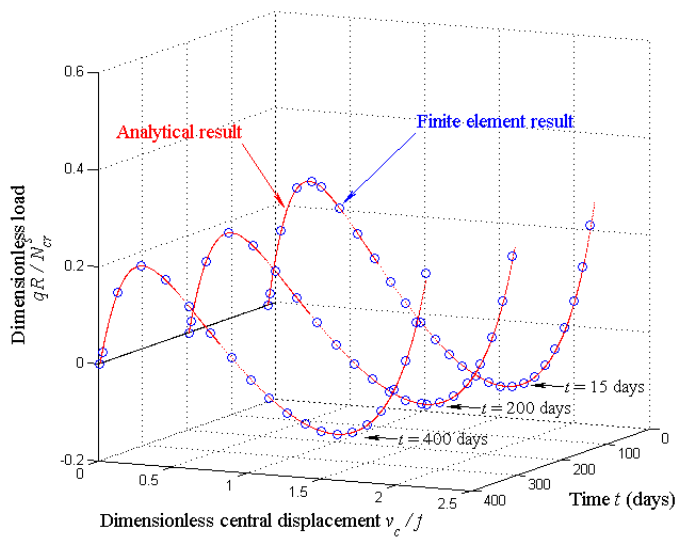

Fig. 7 Comparison with finite element results

Because the buckling of three-pinned CFST arches occurs at the limit points, the positions of these limit points at the non-linear equilibrium paths can be derived by routine calculus. For this, from the definition of the dimensionless load P given by Eq. (25) and the equation of equilibrium given by Eq. (29), the uniform radial load q can be expressed as an implicit function of the time-dependent axial force parameter β_e as $F(q, \beta_e) = 0$. The non-linear equation of equilibrium between the internal force parameter β_e and the dimensionless load P at the limit points needs to satisfy the following equation (Pi *et al*. 2002)

$$\frac{\mathrm{d}q}{\mathrm{d}\beta_e} = -\frac{\partial F(q,\beta_e)/\partial\beta_e}{\partial F(q,\beta_e)/\partial q} = 0\,, \tag{36}$$

which leads to the non-linear equation of equilibrium between μ_e and P at the limit points as

$$A_2P^2 + B_2P + C_2 = 0\,, \tag{37}$$

where the coefficients A_2, B_2, and C_2 are given by

$$A_2 = 2A_1 - \frac{\beta_e \partial A_1}{2\partial\beta_e}, \quad B_2 = 4A_1 \quad \text{and} \quad C_2 = B_1 - \frac{\beta_e^{\,2}}{\lambda_e^{\,2}}\,. \tag{38}$$

The long-term limit point buckling load of a three-pinned CFST arch at a given time t can be obtained by solving Eqs. (29) and (36) simultaneously and the buckling loads so obtained are also shown in Figs. 6 and 7.

The dimensionless non-linear long-term buckling loads qR/N_{cr}^{s} for a group of arches (S = 14.16 m and S/r_e = 100) with different included angles 2Θ are compared with their short-term counterparts loads in Fig. 8, where the short-term buckling loads were determined at t =15 days while the long-term buckling loads were determined at t = 400 days. It can be seen that in the long-term, non-linear analysis predicts significant reductions of the in-plane buckling loads of three-

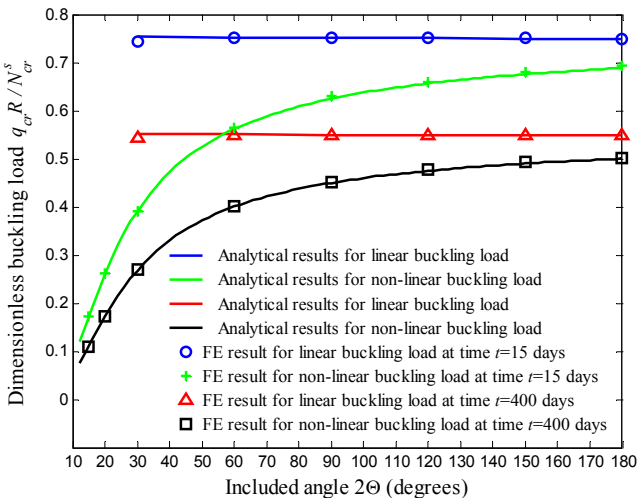

Fig. 8 Short-term and long-term buckling loads of three-pinned CFST arches

pinned CFST arches. Hence, a three-pinned CFST arch that satisfies the stability limit state in the short-term may lose its stability in the long-term and fail by creep buckling.

In order to investigate the importance of geometric nonlinearity in the long-term buckling analysis, the linear short-term and long-term buckling loads of these CFST arches given by Eq. (20) are also shown in Fig. 8. It can be seen that the non-linear buckling loads buckling loads are much lower than their linear counterparts. This shows again that a three-pinned CFST arch that does not buckle under a sustained load when predicted by linear analysis may buckle when predicted by non-linear analysis. Hence, to predict the long-term buckling loads of three-pinned CFST arches, non-linear analysis is required.

The FE results for the long-term buckling loads obtained from the FE program of Luo *et al.* (2013, 2015) for linear and non-linear buckling loads are also shown in Fig. 8 for verification of the analytical solutions. In the FE analyses, the eigenvalue analysis was used for calculating the linear buckling load while non-linear analysis associated with the Riks method was used for determining the non-linear buckling loads. It can be seen that the agreements between the analytical solutions and FE results are excellent.

5. Comparison with two-pinned CFST arches

The structural difference of three-pinned CFST arches with their two-pinned counterparts is the pin at the crown of the arch. The crown-pin is able to transfer shear forces and normal forces but is unable to resist bending moments, leading to free rotation of the arch segments about the pin. Because of the free rotation at the crown, the distributions of displacements and bending moments along a three-pinned arch are much different from those of its two-pinned counterpart. The typical distributions of the dimensionless non-linear short-term (t = 15 days) and long-term (t = 200 days) radial displacements v/f along the length θ/Θ for a three-pinned CFST arch are compared with those for its two-pinned counterpart in Fig. 9.

It can be seen that the radial displacements of the three-pinned CFST arch are larger than those

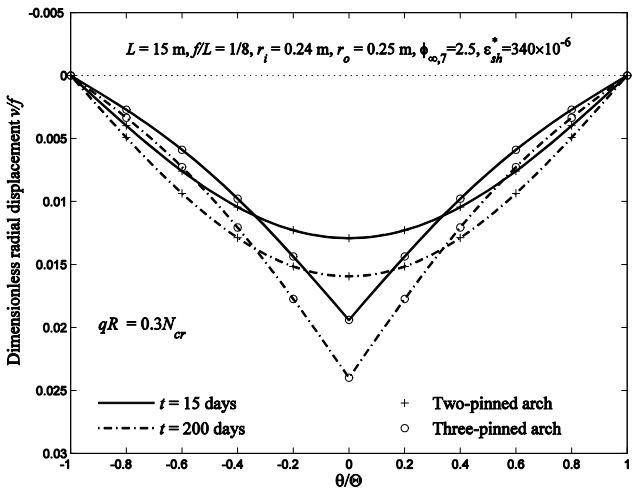

Fig. 9 Comparison of distributions of non-linear long-term radial displacements

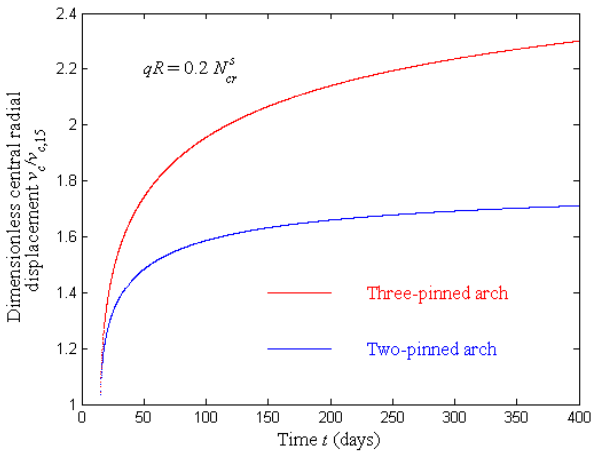

Fig. 10 Comparison of long-term dimensionless central radial displacement $v_c/v_{c,15}$

of the two-pinned arch in their central segments, but are smaller than those in the other segments of arches. It can also be seen that the slope of the two-pinned arch is smooth and vanish at its crown. However, the slope of the three-pinned arch does not continue but has two different limit values at its crown (θ = 0), which depends on whether θ approaches to zero from its positive values or from its negative values. The two different values of slope produce a sharp kink of the radial displacements at the crown, which makes it impossible for the three-pinned arch to bifurcate from symmetric radial displacements to anti-symmetric radial displacements.

In fact, the slope of three-pinned CFST arches can be derived from Eq. (28) as

$$\tilde{v}' = \frac{P}{\mu_e}[\mathrm{H}(\theta)\cos\mu_e\theta\tan\frac{\beta_e}{2} - \sin\mu_e\theta + \mu_e\theta]\Big|_{\theta=0} = \pm\frac{P}{\mu_e}\tan\frac{\beta_e}{2}, \tag{39}$$

while the slope of two-pinned arches can be derived from Pi *et al*. (2011) as

$$\tilde{v}' = \frac{P}{\mu_e}[-\frac{\sin\mu_e\theta}{\cos\beta_e} + \mu_e\theta]\Big|_{\theta=0} = 0. \tag{40}$$

The long-term deformation behaviour of a three-pinned CFST arch is compared with that of a two-pinned counterpart in Fig. 10 as variations of the long-term dimensionless central radial displacement $v_c/v_{c,15}$ with time t. It is clear that the long-term radial displacements of the three-pinned arch are larger than those of the two-pinned arch over the entire time history, for example, at t = 50 days and t = 400 days, $v_c/v_{c,15} \approx 1.74$ and 2.30 for the three-pinned arch while $v_c/v_{c,15} \approx 1.48$ and 1.71 for the two-pinned arch.

The long-term bending behaviour of three-pinned CFST arches is also much different from that of two-pinned CFST arches. Typical comparisons of the distribution of the dimensionless non-linear long-term bending moments $8M/qS^2$ along the length θ/Θ of the three-pinned and two-pinned arches are shown in Fig. 11. It can be seen that the uniform radial load produces negative bending moments in the three-pinned arch because of the crown pin, but positive bending

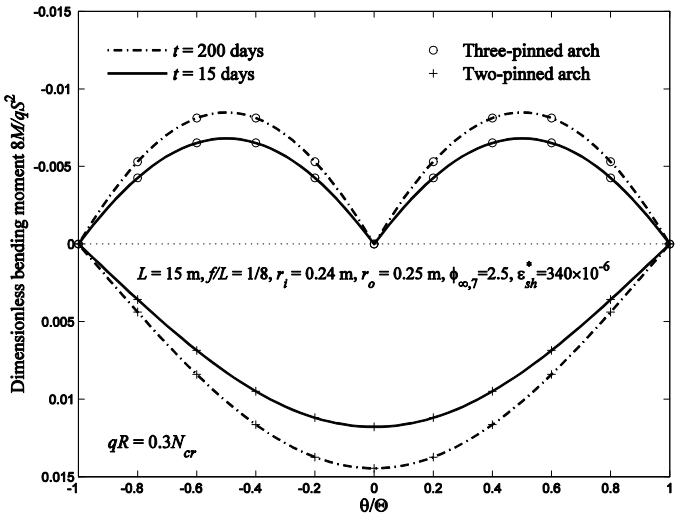

Fig. 11 Distributions of non-linear long-term bending moments

moments in the two-pinned arch. The magnitudes of the bending moments in the three-pinned arch are smaller than those in the two-pinned arch. The maximum bending moments occur at the quarter point of the three-pinned arch, but at the mid-span of the two-pinned arch.

Furthermore, because of the pin at the crown, the long-term in-plane buckling behaviour of three-pinned CFST arches is different from that of two-pinned arches in three aspects. Firstly, two-pinned CFST arches may buckle in a symmetric limit point buckling (snap-through) mode or in an anti-symmetric bifurcation mode as shown by Pi *et al.* (2011). However, because the radial displacements of a three-pinned arch have a sharp kink at its crown (Figs. 4(a) and 9), the sharp kink and free rotation at the crown prevent the symmetric radial displacements from bifurcating to anti-symmetric ones. Hence, the three-pinned CFST arch can buckle only in a symmetric snap-

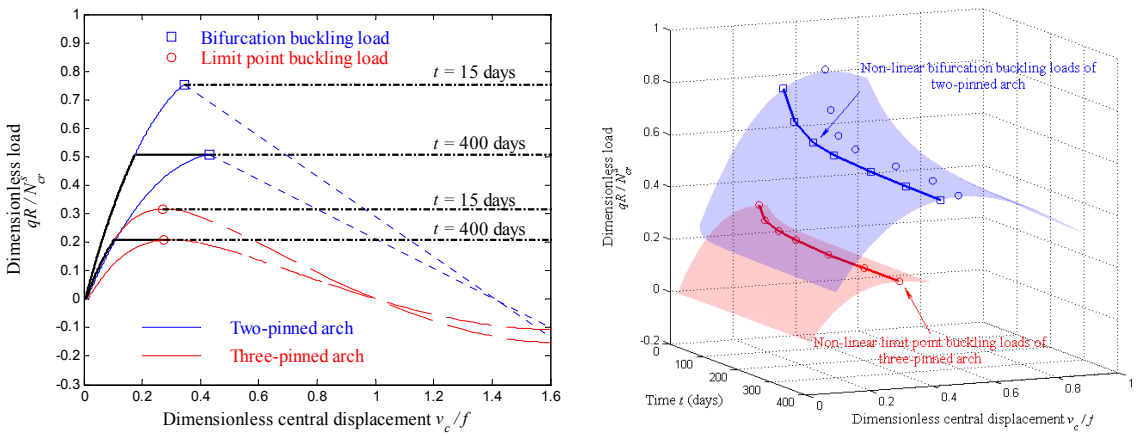

(a) Buckling modes comparisons (b) Comparison of long-term buckling load

Fig. 12 Comparisons of long-term buckling between three-pinned and two-pinned CFST arches

through mode, but not in an anti-symmetric bifurcation mode as shown in Fig. 12(a). Secondly, the non-linear buckling theory can predict the long-term in-plane buckling loads of shallow two-pinned CFST arches accurately but cannot predict the long-term in-plane buckling loads of deep two-pinned CFST arches correctly as shown by Pi *et al*. (2011). However, the non-linear buckling theory can predict the long-term in-plane buckling loads of both shallow and deep three-pinned CFST arches accurately as shown in Fig. 8. Finally, under the same sustained load, a three-pinned CTST arch may buckle in the long-term, but the corresponding two-pinned CFST arch with the same length and included angle cannot buckle as shown in Fig. 12a. For example, under the load $qR = 0.2095\, N_{cr}^{s}$, the three-pinned CFST arch buckles at time $t = 400$ days, while the two-pinned arch does not buckle (Fig. 12(a)). Under the same loading time history, the long-term buckling loads of three-pinned CFST arches are smaller than those of two-pinned CFST arches as shown in Fig. 12(b).

6. Conclusions

Analytical solutions for non-linear long-term deformations and buckling loads of three-pinned CFST circular arches under a sustained uniform radial load were derived. For comparison, the conventional linear analyses for the long-term structural behaviour and buckling were also carried out. It has been found that the geometric nonlinearity influences the long-term behaviour of three-pinned CFST arches significantly. When the geometric nonlinearity is not considered, much small long-term deformations and no long-term internal force changes are predicted. The non-linear analysis has shown that the long-term deformations are larger than the short-term deformations, which significantly reduces the reserve of serviceability limit state. It has also been found that geometric nonlinearity together with the shrinkage and creep of the concrete core reduces the long-term in-plane buckling load of three-pinned CFST arches and that the non-linear analysis predicts much lower long-term in-plane buckling load than the conventional linear analysis. Hence, in the long-term, the three-pinned CFST arches are susceptible to the non-linear in-plane buckling if the sustained load is sufficiently high. It can be concluded that the conventional linear long-term analyses cannot predict the long-term structural behaviour and buckling correctly. To predict the long-term structural behaviour of three-pinned CFST arches and to assess their stability correctly and accurately, the non-linear analyses are required. The long-term behaviour and stability of three-pinned CFST arches were also compared with those of two-pinned CFST arches. It has been shown that the pin at the crown has significant influences on the long-term structural responses of CFST arches. The long-term deformations, the internal actions, and the buckling modes and loads of three-pinned CFST arches are quite different from those of two-pinned CFST arches. This paper provides an in-depth understanding of the non-linear long-term structural responses and buckling of three-pinned CFST arches. The analytical solutions obtained in this paper are useful for structural engineers to assess the non-linear long-term serviceability and stability of three-pinned CFST arches.

Acknowledgments

This work has been supported by the Australian Research Council through a Discovery Project (No. DP140101887) awarded to second and third authors and by the China Scholarship Council through a scholarship (No. 2011695002) awarded to the first author.

References

ACI (1982), Prediction of Creep, Shrinkage and Temperature Effects in Concrete Structures, ACI Committee-209, American Concrete Institute (ACI), Detroit, MI, USA.

Ahmed, E. and Sobuz, H.R. (2011), "Experimental study on long-term behaviour of CFRP strengthened RC beams under sustained load", *Struct. Eng. Mech., Int. J.*, **40**(1), 105-120.

Al-Deen, S., Ranzi, G. and Uy, B. (2015), "Non-uniform shrinkage in simply-supported composite steel-concrete slabs", *Steel Compos. Struct., Int. J.*, **18**(2), 375-394.

ANSYS (2012), Multiphysics 12.1. Ansys Inc., Canonsburg, PA, USA.

AS3600 (2009), Australia Standard: Concrete Structures, Standard Association of Australia, Sydney, Australia.

Aslani, F. (2015), "Creep behaviour of normal- and high-strength self-compacting concrete", *Struct. Eng. Mech., Int. J.*, **53**(5), 921-938.

Au, F.T.K. and Si, X.T. (2012), "Time-dependent effects on dynamic properties of cable-stayed bridges", *Struct. Eng. Mech., Int. J.*, **41**(1), 139-155.

Bazant, Z.P. and Cedolin, L. (2003), *Stability of Structure*, Dover Publications, Mineola, NY, USA.

Bradford, M.A., Pi, Y.L. and Qu, W.L. (2011), "Time-dependent in-plane behaviour and buckling of concrete-filled steel tubular arches", *Eng. Struct.*, **33**(5), 1781-1795.

Chung, K.S., Kim, J.H. and Yoo, J.H. (2013), "Experimental and analytical investigation of high-strength concrete-filled steel tube square columns subjected to flexural loading", *Steel Compos. Struct., Int. J.*, **14**(2), 133-153.

Geng, Y., Ranzi, G., Wang, Y.Y. and Zhang, S. (2012), "Time-dependent behaviour of concrete-filled steel tubular columns: analytical and comparative study", *Magaz. Concrete Res.*, **64**(1), 55-69.

Gilbert, R.I. and Ranzi, G. (2011), *Time-Dependent Behaviour of Concrete Structures*, Spon, London, UK.

Han, L.H., Yang, Y.F. and Liu, W. (2004), "The behaviour of concrete-filled steel tubular columns with rectangular section under long-term loading", *J. Civil Eng.*, **37**(3), 12-18.

Han, B., Wang, Y.F., Wang, Q. and Zhang, D.J. (2013), "Creep analysis of CFT columns subjected to eccentric compression loads", *Comput. Concrete, Int. J.*, **11**(4), 291-304.

Han, L.H., Li, W. and Bjorhovde, R. (2014), "Developments and advanced applications of concrete-filled steel tubular (CFST) structures: Members", *J. Construct. Steel Res.*, **100**, 211-228.

Ichinose, L.H., Watanabe, E. and Nakai, H. (2001), "An experimental study on creep of concrete filled steel pipes", *J. Construct. Steel Res.*, **57**(4), 453-466.

Luo, K., Pi, Y.L., Gao, W. and Bradford, M.A. (2013), "Creep of concrete core and time-dependent non-linear behaviour and buckling of shallow concrete-filled steel tubular arches", *CMES-Comput. Model. Eng. Sci.*, **95**(1), 32-58.

Luo, K., Pi, Y.L., Gao, W., Bradford, M.A. and Hui, D. (2015), "Investigation into long-term behaviour and stability of concrete-filled steel tubular arches", *J. Construct. Steel Res.*, **104**, 127-136.

Ma, Y.S. and Wang, Y.F. (2013), "Creep effects on the reliability of a concrete-filled steel tube arch bridge", *J. Bridge Eng.*, **18**(10), 1095-1104.

Ma, Y.S., Wang, Y.F. and Mao, Z.K. (2011), "Creep effects on dynamic behavior of concrete filled steel tube arch bridge", *Struct. Eng. Mech., Int. J.*, **37**(3), 321-330.

Mias, C., Torres, L., Turon, A. and Sharaky, I.A. (2013), "Effect of material properties on long-term deflections of GFRP reinforced concrete beams", *Construct. Build. Mater.*, **41**, 99-108.

Mirza, O. and Uy, B. (2010), "Finite element model for the long-term behaviour of composite steel-concrete push tests", *Steel Compos. Struct., Int. J.*, **10**(1), 45-67.

Naguib, W. and Mirmiran, A. (2003), "Creep modeling for concrete-filled steel tubes", *J. Construct. Steel Res.*, **59**(11), 1327-1344.

Pi, Y.L., Bradford, M.A. and Uy B. (2002), "In-plane stability of arches", *Int. J. Solid. Struct.*, **39**, 105-125.

Pi, Y.L., Bradford, M.A. and Qu, W.L. (2011), "Long-term non-linear behaviour and buckling of shallow concrete-filled steel tubular arches", *Int. J. Non-linear Mech.*, **46**(9), 1155-1166.

Ranzi, G., Al-Deen, S., Ambrogi, L. and Uy, B. (2013), "Long-term behaviour of simply-supported post-

tensioned composite slabs", *J. Construct. Steel Res.*, **88**, 172-180.
Schmidt, R. (1979), "Initial postbuckling of three-hinged circular arch", *J. Appl. Mech.*, **46**(4), 954-955.
Shao, X., Peng, J., Li, L., Yan, B. and Hu, J. (2010), "Time-dependent behavior of concrete-filled steel tubular arch bridge", *J. Bridge Eng.*, **15**(1), 98-107.
Sundarraja, M.C. and Ganesh Prabhu, G. (2013), "Flexural behaviour of CFST members strengthened using CFRP composites", *Steel Compos. Struct., Int. J.*, **15**(6), 623-643.
Terrey, P.J., Bradford, M.A. and Gilbert, R.I. (1994), "Creep and shrinkage of concrete in concrete-filled circular steel tubes", *Proceeding of 6th International Symposium on Tubular Structures*, Melbourne, Australia, December.
Uy, B. (2001), "Static long-term effects in short concrete-filled steel box columns under sustained loading", *ACI Struct. J.*, **98**(1), 96-104.
Wang, T., Bradford, M.A. and Gilbert, R.I. (2005), "Creep buckling of shallow parabolic concrete arches", *J. Struct. Eng. ASCE*, **132**(10), 1641-1649.
Wang, Y., Geng, Y. Ranzi, G. and Zhang, S. (2011), "Time-dependent behaviour of expansive concrete-filled steel tubular columns", *J. Construct. Steel Res.*, **67**(3), 471-483.

DL